ACS APPLIED MATERIALS & INTERFACES

Research Article

www.acsami.org

Templating Effect of Mesostructured Surfactant–Silica Monolithic Films on the Surface Structural and Mechanical Properties

Motohiro Tagaya,*[,†] Nobutaka Hanagata,[‡] and Takaomi Kobayashi[†]

[†]Department of Materials Science and Technology, Nagaoka University of Technology, 1603-1 Kamitomioka, Nagaoka, Niigata 940-2188, Japan

[‡]Nanotechnology Innovation Station, National Institute for Materials Science (NIMS), 1-2-1 Sengen, Tsukuba, Ibaraki 305-004, Japan

Supporting Information

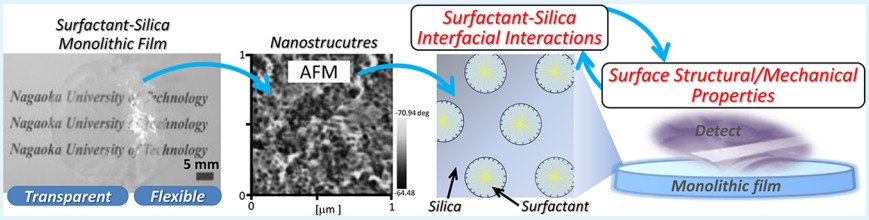

ABSTRACT: Mesostructured surfactant–silica monolithic films were prepared using a supramolecular templating method. The effect of the templating in the monolithic films on the interfacial interactions was evaluated and elucidated using the atomic force microscope techniques combined with other surface analyses to produce different surface structures and force curves depending on the surfactants. The transparent and flexible surfactant–silica monolithic films were prepared to exhibit the ordered nanostructures. The monolithic films templated by nonionic triblock copolymers (poly(ethylene oxide (EO))–poly(propylene oxide (PO))–poly(ethylene oxide (EO))) of $EO_{20}PO_{70}EO_{20}$ (P123) and $EO_{106}PO_{70}EO_{106}$ (F127) significantly exhibited flat surfaces and the higher viscoelastic properties which were supported by surface stiffness and adhesive force, whereas the monolithic film by cationic alkylammonium surfactant indicated a rough surface and the plastic deformation property by application of force. This indicated that the higher molecular weight of the EO and PO phases enhanced the phase segregation in the silica surfaces due to the higher solubility differences between both blocks to consolidate the surfactant–silica interfacial interactions. Therefore, the different surface structural and mechanical properties attributed to the interfacial organic–inorganic interaction patterns were successfully clarified.

KEYWORDS: *organic–inorganic nanocomposites, nonionic surfactants, monolithic films, mesoporous silicas, atomic force microscopy*

1. INTRODUCTION

The synthesis, characterization, and applications of mesostructued materials have been extensively investigated after the discovery of mesoporous silicas prepared by the cooperative organization of surfactants and inorganic species.[1,2] The organic–inorganic nanocomposites synthesized by supramolecular templating methods were used as the host to produce the functional host–guest complexes,[3−9] and the possible applications for photofunctional and biofunctional materials have been recently studied.[10−13] The preparation of the mesostructured composites using the surfactant assemblies to react with inorganic species has attracted increasing interest in order to understand biomimetic hierarchical mesostructures, such as the surfactant–inorganic biphasic arrays,[14−18] suggesting the importance of the basic research on the surfactant–inorganic interfacial interactions.

Various surfactants have been used for the mesostructure formation. Quaternary ammonium surfactants (e.g., hexadecyltrimethylammonium) were used as the typical templates,[1] and the other surfactants, such as alkylamines[19,20] and poly(ethylene oxide),[21] have been used to precisely control the mesostructures. An amphiphilic triblock copolymer (TBC), for example, poly(ethylene oxide (EO))–poly(propylene oxide (PO))–poly(ethylene oxide (EO)), was also used as the template to produce the mesostructures with larger nanopores. Because of the variety in both mesostructural and macroscopical morphologies,[22−25] and the improvement of their mechanical properties, the understanding of the template dependence on the interfacial phenomena is of great interest.

The processing of the mesostructured surfactant–silica materials into a controlled morphology is a basic prerequisite for optics, separations, catalytic, and sensing applications. Accordingly, the preparation of the macroscopic morphologies, such as films,[28−34] hollow and hard spheres,[35−37] fibers,[38] and monoliths[39,40] of the mesostructures, has been researched. Among all these morphologies, the silica–surfactant monolithic films with a bulk size are especially ideal host materials for such applications,[41,42] since the nanoscale mesostructured mono-

Received: August 25, 2012
Accepted: October 22, 2012
Published: October 22, 2012

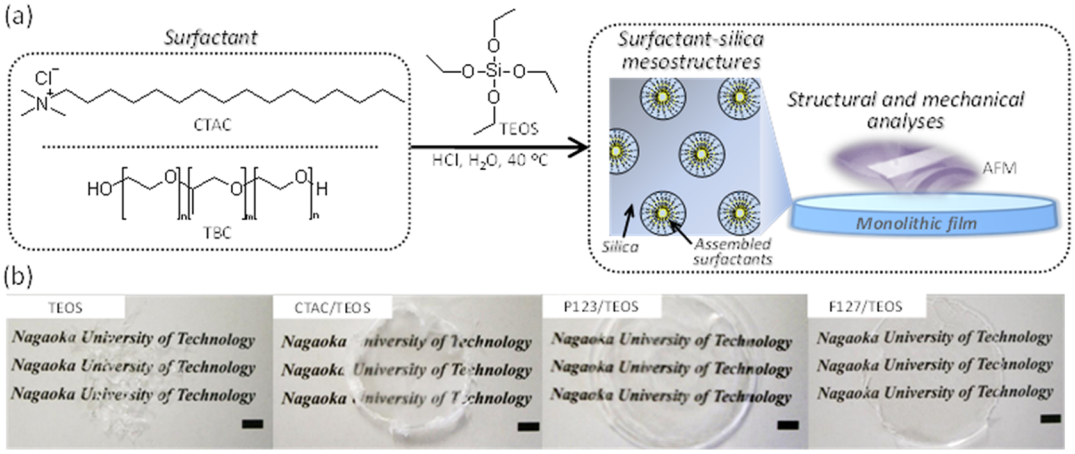

Figure 1. (a) Scheme of the structural and mechanical analyses of the surfactant-silica mesostructured monolithic film prepared by the supramolecular templating method using the surfactants (CTAC and TBC (n = 20 and m = 70 for P123 and n = 106 and m = 70 for F127)) and TEOS and (b) the photographs of the monolithic films with the different templates (scale bar: 5 mm).

lithic film surfaces are thought to display a handling ability and the characteristic viscoelastic behavior. As the practical challenges, an analysis and evaluation of the interfacial interactions between the silica walls and templated surfactants should be researched for improving the structural and mechanical properties at a bulk state. However, the analytical investigation of the interfacial phenomena in the monolithic films has not been investigated and reported. Thus, the characterization at the connective interfaces of the mesostructures based on the interactions as well as the well-defined structures is very important.

In this study, the surface structural and mechanical properties of the preparative surfactant−silica mesostructured monolithic films depending on the surfactant template were examined using an atomic force microscope (AFM) combined with other surface analyses as shown in Figure 1a, which have emerged as useful tools to determine the interfacial physicochemical properties. Furthermore, the interactions between the surfactants (cetyltrimethylammonium chloride (CTAC) and TBC) and the silica from tetraethoxysilane (TEOS) in the mesostructured nanocomposites were investigated by the nanomechanical analysis in order to clarify the template effect on the surface properties.

2. EXPERIMENTAL SECTION

Materials. Ethanol (99.5 vol %) and hydrochloric acid (HCl) as special grade chemicals were purchased from Wako Chemical Co., Ltd. Hexadecyltrimethylammonium chloride (CTAC) and tetraethylorthosilicate (TEOS) as shown in Figure 1a as first reagent grade were purchased from Tokyo Kasei Ind. Co., Ltd. The triblock copolymers (TBCs) of poly(ethylene oxide)−poly(propylene oxide)−poly(ethylene oxide) as P123 ($EO_{20}PO_{70}EO_{20}$; M_W = 5800) and F127 ($EO_{106}PO_{70}EO_{106}$, M_w = 12 600) were purchased from Aldrich Co., Ltd. All chemicals were used as received without purification, and ultrapure water was used in all the experiments.

Preparation of Monolithic Films. The monolithic film as the template of CTAC was synthesized according to a previous report.[45] A 6.9 g sample of CTAC was dissolved into 28 mL of an HCl aqueous solution (pH = 1.8) and stirred for 30 min. A 2 mL portion of TEOS was added to the solution and stirred at 40 °C for 2 h.

The monolithic film as the template of P123 was synthesized according to a previous report.[46] A 0.90 g sample of P123 was dissolved in 15 mL of ethanol and stirred for 30 min. A 0.1 sample g of an HCl aqueous solution (2 N) and 0.80 g of water were added to the solution, and stirred for 30 min. A 2 mL portion of TEOS was then added to the solution and stirred at 40 °C for 2 h.

The monolithic film as the template of F127 was synthesized according to a previous report.[47] A 0.94 g sample of F127 was dissolved in 6.8 mL of ethanol, and stirred for 30 min. A 1.4 mL of an HCl aqueous solution (pH = 1.4) was added to the solution and stirred for 30 min. A 2 mL portion of TEOS was then added to the solution and stirred at 40 °C for 2 h.

As a reference, the siliceous film using only TEOS as the template-free was synthesized. A 1.4 mL portion of an HCl aqueous solution (pH = 1.4) was dissolved into 6.8 mL of ethanol and stirred for 30 min; 2 mL of TEOS was then added to the solution and stirred at 40 °C for 2 h.

All the resulting solutions were transferred to Teflon vessels (bottom area: 7.9 cm^2) at the solution density of 0.4 mL/cm^2, stored and aged at room temperature for 3 days in order for allow gelation, then dried at 60 °C for 18 h, and peeled from the vessels to obtain the self-standing monolithic films. The monolithic films without and with the surfactants of CTAC, P123, and F127 were abbreviated as TEOS, CTAC/TEOS, P123/TEOS, and F127/TEOS, respectively. In order to measure X-ray diffraction (XRD) patterns and BET surface area of the mesopores after removal of the surfactants, the templates in these resulting solids were completely removed by calcination in air at 823 K for 8 h at a heating rate of 10 K min^{-1}, as confirmed by the Fourier transform infrared (FT-IR) spectra.

Characterization. The UV−visible transmittance was measured using a UV−vis-NIR spectrophotometer (V-570; JASCO Co., Japan), and the total transmittance was calculated by the average transmittance in the wavelength range at 400−800 nm. The surface wettability was analyzed in air by the sessile drop method of distilled water using a contact angle meter (CA-W200, Kyowa Interface Science, Inc.). The droplet was controlled at the volume of 1.5 mL using a dripping nozzle, and the initially attached area on the substrate surfaces was 1.6 mm^2 when approaching the nozzle to the surfaces. The FT-IR spectra were recorded by an FT-IR spectrometer (Prestige-21; Shimadzu Corp., Japan) in the transmittance mode and were obtained using a KBr method at a resolution of 4 cm^{-1}. The XRD patterns were recorded by a X'Pert Pro MPD (PNAalytical Co., Ltd.) using monochromatized Cu Kα radiation. The morphologies were observed using a field emission scanning electron microscope (FE-SEM: Hitachi Co., Ltd., S-4500N) at 20 kV. Nitrogen adsorption and desorption isotherms were measured at 77 K by a SA3100 instrument (BECHMAN COULTER Co., Ltd.) to calculate the BET surface area and averaged pore size. Prior to the measurement, the samples were degassed under vacuum at 393 K for 4 h.

The nanostructures and surface viscoelastic properties were analyzed by an atomic force microscope (AFM; Nanocute, SII Investments, Inc.) in an area of 1.0 × 1.0 μm^2. A silicon probe

mounted on a cantilever (SII Micro Cantilever SI-AF01, SII Investments, Inc.) was employed. The surface roughness (R_{rms}) was calculated by the root mean squares in the Z-range images.

The force curves[43,44] were measured at the scan rate of 30 nm/s and displacement sensitivity of 40 mV/nm. The schemes of the force curve measurement as a function of the distance between the probe tip and sample surfaces and the interfacial interactive structures are shown in Scheme 1. At a large separation in Scheme 1I, the interactions between the tip and sample surface are negligible as such that the spring cantilever remains in an undeflected state. As the sample approaches the tip, the interactions between the tip and sample surfaces at a certain separation cause a deflection of the spring cantilever upward or downward, depending on the nature of the force. With a further approach to each other in Scheme 1II, the interfacial forces increase in magnitude until the cantilever irreversibly jumps and contacts the sample surface. From this point onward, the cantilever and sample move together until reaching its set upward limit. The decline in the saturated region in the approaching curve was calculated in order to understand the nanomechanical properties. The tip−sample stiffness, S, can be represented by eq 1.[48]

Scheme 1. Scheme of the Force Curves As a Function of the Distance between the Probe Tip and Sample Surface, Which Indicates the Different Interfacial Interactions at the Position I−IV as described in the Experimental Section

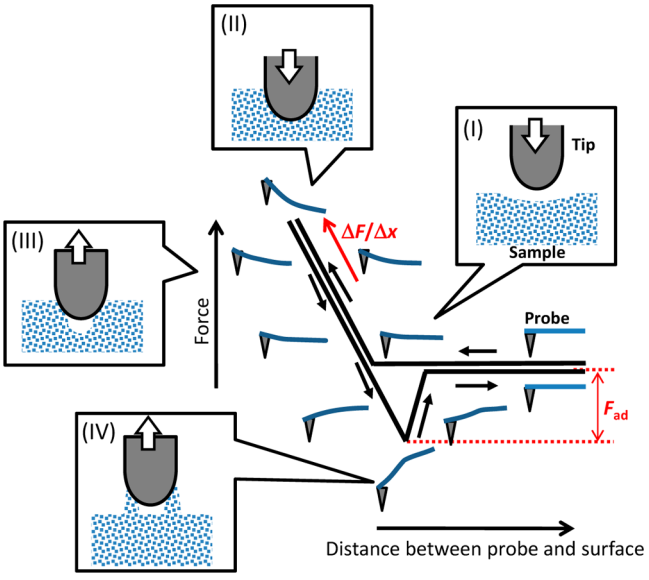

$$S = (\Delta F/\Delta x) - k \quad (1)$$

where k is the spring constant of the cantilever and is considered to be 0.2 nN/nm. ΔF is the modulated force, and Δx is the amplitude of the tip on the sample. The decline of the region in the curves is shown in Scheme 1. Furthermore, S can be also represented by eq 2.[48,49]

$$S = 2aE^* \quad (2)$$

where a is the contact radius onto the monolithic film, which is estimated to be ca. 20 nm according to the tip radius used in this study. On the basis of eqs 1 and 2, E^*, which is the Young's modulus of the monolithic film, was also calculated. The sample subsequently retracts back in Scheme 1III. If there is an adhesion force (F_{ad}) between the tip and the sample, the sample will pull the tip downward as it retracts until the restoring force of the cantilever spring exceeds the adhesion force at which time the cantilever jumps back to its normal position as shown in Scheme 1IV. The F_{ad} in the curve was defined along the force axis as shown in Scheme 1. The value for the CTAC/TEOS film was calculated only by the approaching curve due to the plastic deformation behavior, and those for the other surfaces by the retracting curve. As a result, one force probing cycle is completed.

All the measurements were repeatedly conducted five times to obtain the average values. The statistical analysis of all the measurements was evaluated using the student's t test.

3. RESULTS AND DISCUSSION

As shown in Figure 1b, the surfactant−silica monolithic films with the different templates were in a transparent and self-standing state with a length up to several centimeters while preserving the vessel shape, whereas TEOS alone was in a the fragmented state, suggesting that the nanocomposite structures by the silica frameworks combined with the surfactant functional groups enhance and stabilize the interfacial interactions. The monolithic films have thicknesses of several hundred micrometers (TEOS ca. 250 μm, CTAC/TEOS ca. 180 μm, P123/TEOS ca. 200 μm, F127/TEOS ca. 250 μm) and transparency, and the total transmittance of the F127/TEOS is almost the same as that of TEOS alone as shown in the Table 1, indicating the ordered structures at a nanoscale to reduce the visible-light scattering. Thus, the macroscopic properties of the monolithic films significantly depended on the templating surfactants.

Figure S1 shows the FT-IR spectra of the monolithic films with the different templates (see the Supporting Information). In all the spectra, the characteristic bands at around 1070 and 1225 cm^{-1} that originated from the Si—O—Si asymmetric and symmetric stretching and the bands at around 960 cm^{-1} assigned to the Si—OH stretching were clearly observed. Furthermore, the surfactant−silica monolithic films indicated that the several bands at around 2850−2950 cm^{-1} can be assigned to the C—H bending of the surfactant molecules, indicating the formation of the surfactant−silica nanocomposite phases. The existence of the surfactants inside the nanochannels could not prevent a capillary-adsorption of the remaining water molecules. As shown in Table 1, the surface wettability of the TBC-templated silicas is higher than those of the TEOS and CTAC/TEOS, indicating that the poly(propylene) hydrophobic block would be partially segregated on the silica surfaces to reduce the surface free energy. In contrast, the water-interactive parts (e.g., cationic group and ≡Si—O^-) would be functionalized on the TEOS and CTAC/TEOS near-surfaces at the higher density. Therefore, the transparent surfactant−silica monolithic films were successfully prepared.

Table 1. Surface Properties (Total Transmittance, Contact Angle, Roughness (R_{rms}), Stiffness (S), Adhesive Force (F_{ad})) of the Monolithic Films

sample	total transmittance (%)	contact angle (degree)	R_{rms} (nm)	S (nN/nm)	F_{ad} (nN)
TEOS	62.6	10.1 ± 3.21	0.291 ± 0.050	1.31 ± 0.030	3.30 ± 0.230
CTAC/TEOS	21.2	14.1 ± 3.23	17.8 ± 4.43		
P123/TEOS	42.3	31.5 ± 2.51	3.36 ± 0.87	1.71 ± 0.060	4.76 ± 0.390
F127/TEOS	53.9	34.3 ± 4.54	2.37 ± 1.21	5.63 ± 0.390	21.0 ± 4.36

dx.doi.org/10.1021/am301789v | ACS Appl. Mater. Interfaces 2012, 4, 6169−6175

Figure 2a shows the FE-SEM images of the monolithic films with the different templates. TEOS alone showed winding

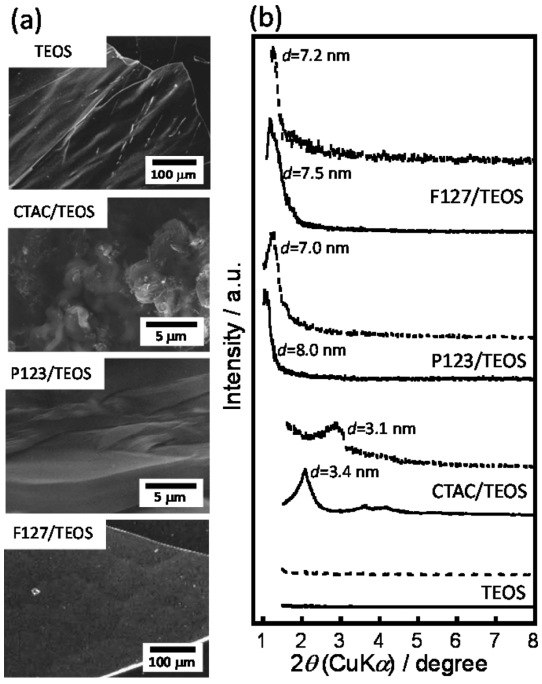

Figure 2. (a) FE-SEM images of the monolithic films with the different templates and (b) the XRD patterns at a lower angle: (solid lines) as-prepared, (dashed lines) after the calcination of the as-prepared samples.

surfaces with the period of several tens of micrometers that were formed by the stress during the dry process, while the CTAC/TEOS showed a particulate morphology with the size of several micrometers. In the TBC, there is little to distinguish P123 from F127; the cross-sectional images indicated the layered structures as shown in the P123/TEOS, and the near-surfaces of the monolithic films exhibited the scale-like morphologies with the period of several tens of micrometers and had flat surfaces as shown in the F127/TEOS. Therefore, the different morphologies depending on the templates were observed, which would be attributed to the interfacial surfactant−silica interactions.

Figure 2b shows the XRD patterns of the monolithic films with the different templates. TEOS alone did not exhibit the ordered arrangements. In the surfactant−silica monolithic films, the significant diffraction peaks at the lower angles before and after the calcination are observed. With the calcination, the diffraction patterns were shifted to the higher angles due to the silica framework contraction. The apparent diffraction of the TBC/TEOS was detected by the calcination, indicating the TBC−silica mesostructures with larger periodic sizes. In the wide-angle range, there are no detectable diffractions due to any impurities (e.g., surfactant phases). These results indicated the successful formation of the surfactant−silica mesostructures in the monolithc films. Furthermore, the nitrogen adsorption/desorption isotherms of the monolithic films after the calcination showed the BET surface areas of 675, 519, and 614 m^2/g silica for the CTAC/TEOS, P123/TEOS, and F127/TEOS, respectively. These isotherms are classed as type IV, indicating the presence of mesopores after the calcination. Moreover, the pore sizes of 2.6, 5.0, and 5.7 nm for the CTAC/TEOS, P123/TEOS, and F127/TEOS were confirmed by the pore size distribution derived from the nitrogen adsorption isotherms. According to these results, the silica wall widths and the assembled surfactant sizes confined by the walls of the as-prepared monolithic films are approximately 0.5−1 and 2−3 nm for CTAC/TEOS and 1−2 and 5−6 nm for TBC/TEOS. Thus, it was suggested that the templated surfactants in the silica frameworks combined with the functional groups of the surfactants to rearrange the Si−O−Si network and form the ordered mesostructures.

Figure 3 show the AFM topographic and phase-shift images of the monolithic films with the different templates at the

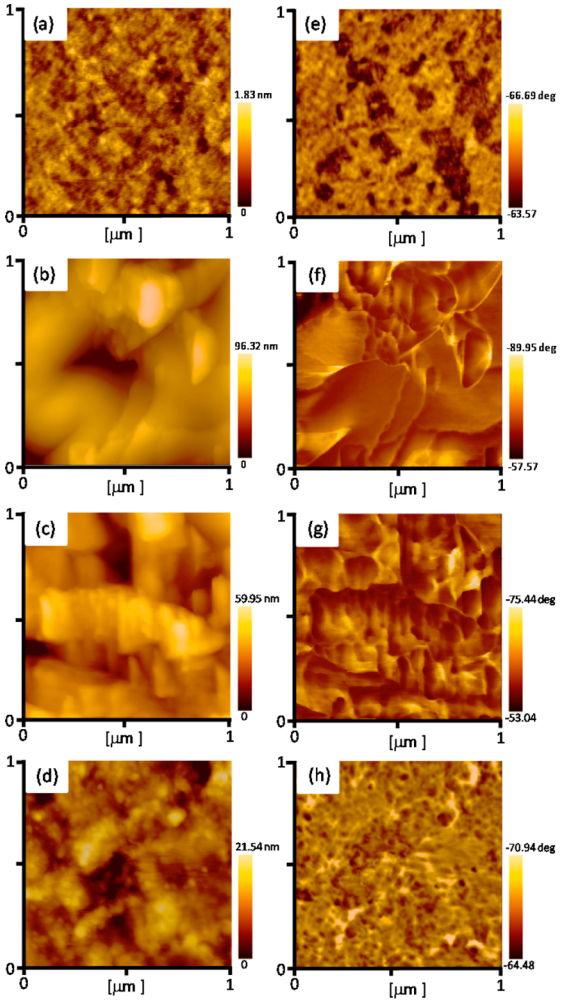

Figure 3. AFM (a−d) topographic and (e−h) phase-shift images of the monolithic films of (a, e) TEOS, (b, f) CTAC/TEOS, (c, g) P123/TEOS, and (d, h) F127/TEOS.

observation area of 1 μm × 1 μm. The TEOS alone showed nanoparticulate surfaces that were flat surface structure (R_{rms} = 0.291 ± 0.050 nm). The CTAC/TEOS that was focused and taken on the particulate surface showed a rough surface (R_{rms} = 17.8 ± 4.43 nm) had the inhomogeneous domains with wider size distribution. The TBC/TEOS had flat surfaces with the R_{rms} values of 3.36 ± 0.87 nm for P123/TEOS and 2.37 ± 1.21 nm for F127/TEOS and the phase-shift images of the TBC/TEOS surfaces were also of uniform brightness, indicating the

dx.doi.org/10.1021/am301789v | ACS Appl. Mater. Interfaces 2012, 4, 6169−6175

formation of homogeneous nanostructures by the TBC−silica nanocomposites.

Figure 4 shows the force curves for the monolithic film surfaces with the different templates. As shown in the

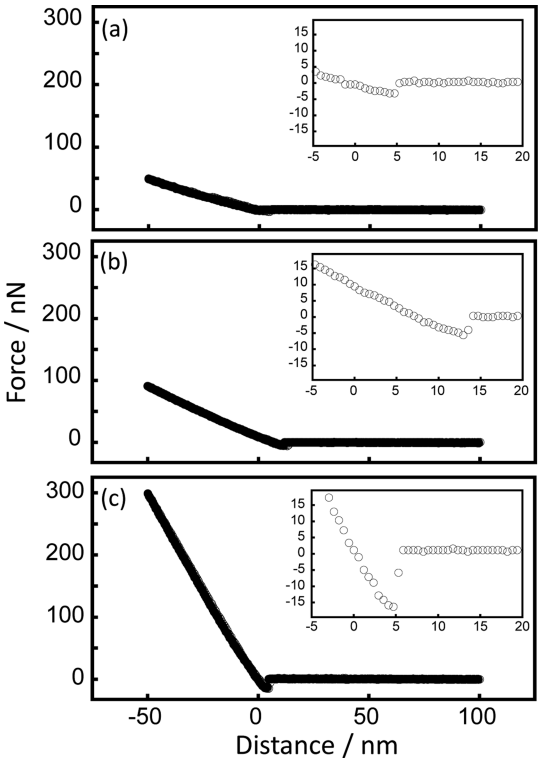

Figure 4. Force curves (• approaching, ○ retracting) of the monolithic film surfaces of (a) TEOS, (b) P123/TEOS, and (d) F127/TEOS. (inset) Magnified retracting curves in the adhesive areas.

Supporting Information, Figure S2, the marks measured in the force curves are indicated in the AFM topographic images. Typical tip−sample interactive behaviors for the TEOS and TBC/TEOS were observed as shown in Figure 4, whereas the CTAC/TEOS exhibited a plastic deformation behavior as shown in Supporting Information Figure S3. The nanocomposite structure of CTAC/TEOS was stabilized by both the electrostatic interactions between ammonium ion and silanol group and the hydrophobic interactions among alkylchains. The assembled micelle structure would be easily broken by the initial approaching interactions to enhance the alkylchains interactions. These results indicate the significant templating effect on the surface viscoelasticity. During the initial stage, there is a measurable attraction between the two at the separation distance below 10 nm; a slight attractive force between the tip and the sample during the approaching process is observed, which is attributed to the interactions between the tip and surfactant−silica. In particular, this strongly appears in the CTAC/TEOS (see Supporting Information Figure S3 inset), suggesting that the cationic CTAC surfactant strongly adsorbs on the SiO_2 probe tip surface.

Subsequently, a repulsion force between the tip and the sample is evident, starting at the distance of around a few nanometers. This is attributed to the overlap of the electric double layers around the two surfaces between the tip and sample surfaces. The S values of the surfactant−silica nanocomposite surfaces are higher than that of the TEOS alone, and the F127/TEOS surface is highest of all the surfaces (Table 1), indicating the importance of the surfactant templating for the mechanical properties. Furthermore, the E^* values of the monolithic films were 33, 35, and 136 MPa for the TEOS, P1223/TEOS, and F127/TEOS, respectively, which approximately corresponds to the polymer materials (e.g., poly(dimethylsiloxane) and poly(urethane)). In the approaching curve of CTAC/TEOS, the S and E^* values were 2.52 ± 0.350 nN/nm and 63 MPa, respectively.

At a separation distance of around a few nanometers in the retracting process, the tip jumps inward and subsequently a maximum F_{ad} is observed. Therefore, it is reasonable to conclude that the monolithic film surfaces interacted with the fragmented surfaces after the insert of the tip, and the F_{ad} of F127/TEOS is the highest of all the surfaces as shown in Table 1, suggesting the favorable interactions (e.g., hydrogen bonding, electrostatic interactions) of the SiO_2 tip surfaces with sample surfaces of both the F127 and TEOS. In the approaching curve of the CTAC/TEOS, the F_{ad} was observed to be the value of 15.1 ± 3.39 nN, indicating that the SiO_2 tip surface strongly interact with the sample surfaces, which would induce the structural rearrangement.

It has been known that two different mechanisms are suggested for the formation process of the mesostructures. In true liquid-crystal templating, the concentration of the surfactant is so high that under the prevailing conditions (temperature, pH), a lyotropic liquid-crystalline phase is formed without requiring the presence of the precursor siliceous framework materials.[26] On the other hand, it is also possible that this phase forms even at lower concentrations of the surfactant molecules, for example, when there is a cooperative self-assembly of the structure-directing agents and the already added siliceous species, in which case, a liquid-crystal phase with ordered arrangements (hexagonal, cubic, or laminar) can develop.[27] In this study, the templated surfactants are cooperatively assembled in the silica framework with well-defined voids of less than ca, 10-nm diameter based on the XRD results, suggesting the occurrence of the surfactant−silica interfacial interactions to form the ordered arrangements.

The organization of the TBC-templated mesostructures depended on the TBC weight fraction to silica.[47] For the lower weight fraction, the nonordered structures were formed due to a relatively strong interaction of the siloxane frameworks forming the siliceous skeleton with both the PEO and PPO blocks. The strong interactions extend the hybrid interactions, hindering PPO segregation. For the higher weight fraction, the PPO/PPO attractions take over the interactions between ≡Si—O^- and PPO, and microsegregation takes place, resulting in a mesostructural order. In all the cases, it is noted that strong interactions are observed between the PEO block and the siliceous networks, so that the end groups (e.g., ≡Si—O^-, ≡Si—O—Si≡) of the siliceous networks thought to be completely integrated into the PEO block to form the three-phases along the interfaces as shown in Scheme 2. These interfacial interactions for the TBC/TEOS would effectively affect the physicochemical properties. In particular, the stiffness of the TBC/TEOS is significantly higher, and that of F127/TEOS is the highest in the monolithic films. Thus, these results indicate that the higher molecular weight of the PEO and PPO phases and the ratio of PEO to PPO of F127 enhanced the integration of TEOS into the PEO block and the phase segregation due to the higher solubility differences between both blocks to consolidate the interfacial interactions, even

Scheme 2. Possible Schemes of the Interfacial Structures in the Surfactant−Silica Nanocomopposites, Which Would Affect the Surface Structural and Mechanical Properties

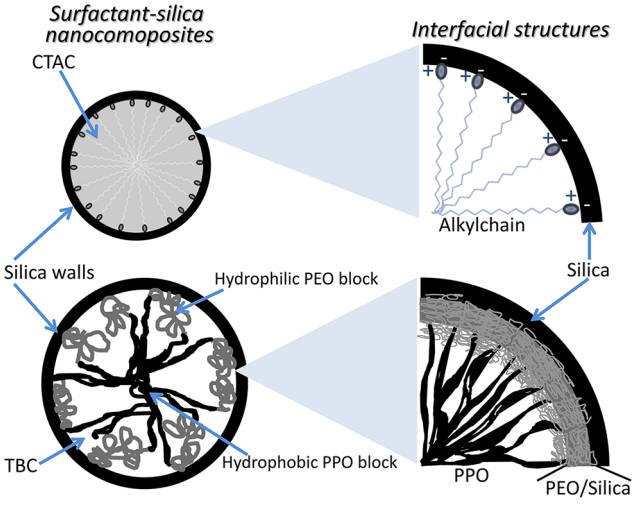

though the hydrophilic/lipophilic balance and shape are changed by the polymerization degree.[50] Furthermore, F127/TEOS has many entanglements due to the copolymer with higher molecular weight to be stabilized by the shorter molecular weight between entanglements. On the other hand, the ordered micelle structure of CTAC/TEOS, which electrostatically interacts with the end groups as shown in Scheme 2, has a little entanglement and fluid property due to liquid crystallinity to easily rearrange the structure by the external force and enhance the hydrophobic interactions among the alkylchains. Therefore, the important advantage and availability of the F127-templating mesostructures as compared to the ordinary cationic surfactant are successfully elucidated based on the surface nanostructural and nanomechanical properties of the monolithic films.

4. CONCLUSIONS

The effect of the templating in the monolithic films on the interfacial interactions was investigated using the AFM techniques combined with other surface analyses. The mesostructured surfactant−silica monolithic films were prepared by templating the different supramolecular surfactants to obtain transparent and self-standing states with a thickness of the several hundred micrometers. The template effect on the interfacial interactions in the monolithic films was successfully evaluated and elucidated. TBC/TEOS significantly exhibits nanoparticulate flat surfaces with ordered nanostructures and higher stiffness values, whereas the CTAC/TEOS has a rough surface and a plastic deformation behavior. These differences were attributed to the surfactant ability as well as the interfacial interactions between the surfactant and silica. It was suggested that the siliceous networks were strongly integrated into the PEO block of TBC to form the strongly interactive phase to consolidate the surfactant−silica interfacial interactions. Therefore, the different surface structural and mechanical properties attributed to the interfacial interaction patterns were successfully clarified, which will be valuable for the application of the mesostructured monolithic films.

■ ASSOCIATED CONTENT

Ⓢ Supporting Information

FT-IR spectra of the monolithic films. AFM topographic images and the numbered marks measured in the force curves. Force curves of CTAC/TEOS. This information is available free of charge via the Internet at http://pubs.acs.org/.

■ AUTHOR INFORMATION

Corresponding Author

*E-mail: tagaya@mst.nagaokaut.ac.jp. Tel.: +81-258-47-9345.

Notes

The authors declare no competing financial interest.

■ ACKNOWLEDGMENTS

This work was partly supported by a Grant-in-Aid for Challenging Exploratory Research (Grant No. 24651133) of MEXT/JSPS KAKENHI. The authors thank Prof. Dr. Makoto Oagawa, Prof. Dr. Junzo Taaka, and Prof. Dr. Toshiyuki Ikoma for many helpful discussions.

■ REFERENCES

(1) Yanagisawa, T.; Shimizu, T.; Kuroda, K; Kato, C. *Bull. Chem. Soc. Jpn.* **1190**, *63*, 988−992.
(2) Kresge, C. T.; Leonowicz, M. E.; Roth, W. J.; Vartuli, J. C.; Beck, J. S. *Nature* **1992**, *359*, 710−712.
(3) Moller, K.; Bein, T. *Chem. Mater.* **1998**, *10*, 2950−2963.
(4) Stein, A.; Melde, B. J.; Schroden, R. C. *Adv. Mater.* **2000**, *12*, 1403−1419.
(5) Scott, B. J.; Wirnsberger, G.; Stucky, G. D. *Chem. Mater.* **2001**, *13*, 3140−3150.
(6) Ogawa, M. *J. Photochem. Photobiol., C Photochem. Rev.* **2002**, *3*, 129−146.
(7) Tagaya, M.; Ogawa, M. *Chem. Lett.* **2006**, *35*, 108−109.
(8) Tagaya, M.; Ogawa, M. *Phys. Chem. Chem. Phys.* **2008**, *10*, 6849−6855.
(9) Tagaya, M.; Motozuka, S.; Kobayashi, T.; Ikoma, T.; Tanaka, J. *J. Mater. Chem.* **2012**, *22*, 18741−18743.
(10) Okuda, M.; Takeguchi, M.; Zhu, Y.; Hashimoto, A.; Ogawa, N.; Tagaya, M.; Chen, S.; Hanagata, N.; Ikoma, T. *Surf. Interface Anal.* **2010**, *42*, 1548−1551.
(11) Tagaya, M.; Ikoma, T.; Yoshioka, T.; Minami, F.; Tanaka, J. *Mater. Lett.* **2011**, *65*, 2287−2290.
(12) Tagaya, M.; Ikoma, T.; Yoshioka, T.; Tanaka, J. *J. Colloid Interface Sci.* **2011**, *363*, 456−464.
(13) Tagaya, M.; Ikoma, T.; Yoshioka, T.; Xu, Z.; Tanaka, J. *Chem. Commun.* **2011**, *47*, 8430−8432.
(14) Inagaki, S.; Fukushima, Y.; Kuroda, K. *J. Chem. Soc., Chem. Commun.* **1993**, 680−682.
(15) Huo, Q.; Margolese, D. I.; Ciesla, U.; Feng, P.; Gier, T. E.; Sieger, P.; Leon, R.; Petroff, P. M.; Schüth, F.; Stucky, G. D. *Nature* **1994**, *368*, 317−321.
(16) Tanev, P. T.; Chibwe, M.; Pinnavaia, T. J. *Nature* **1994**, *368*, 321−323.
(17) Tanev, P. T.; Pinnavaia, T. J. *Science* **1996**, *271*, 1267−1269.
(18) Mann, S.; Ozin, G. A. *Nature* **1996**, *382*, 313−318.
(19) Tanev, P. T.; Pinnavaia, T. J. *Science* **1995**, *267*, 865−867.
(20) Tanev, P. T.; Pinnavaia, T. J. *Chem. Mater.* **1996**, *8*, 2068−2079.
(21) Bagshaw, S. A.; Prouzet, E.; Pinnavaia, T. J. *Science* **1995**, *269*, 1242−1244.
(22) Zhao, D.; Feng, J.; Huo, Q.; Melosh, N.; Fredrickson, G. H.; Chmelka, B. F.; Stucky, G. D. *Science* **1998**, *279*, 548−552.
(23) Zhao, D.; Huo, Q.; Feng, J.; Chmelka, B. F.; Stucky, G. D. *J. Am. Chem. Soc.* **1998**, *120*, 6024−6036.
(24) Fan, J.; Yu, C.; Wang, L.; Tu, B.; Zhao, D.; Sakamoto, Y.; Terasaki, O. *J. Am. Chem. Soc.* **2001**, *123*, 12113−12114.

(25) Yu, C.; Tian, B.; Fan, J.; Stucky, G. D.; Zhao, D. *J. Am. Chem. Soc.* **2002**, *124*, 4556−4557.
(26) Attard, G. S.; Glyde, J. C.; Göltner, C. G. *Nature* **1995**, *378*, 366−368.
(27) Monnier, A.; Schüth, F.; Huo, Q.; Kumar, D.; Margolese, D.; Maxwell, R. S.; Stucky, G.; Krishnamurty, M.; Petroff, P.; Firouzi, A.; Janicke, M.; Chmelka, B. F. *Science* **1993**, *261*, 1299−1303.
(28) Ogawa, M. *J. Am. Chem. Soc.* **1994**, *116*, 7941−7942.
(29) Ogawa, M. *Langmuir* **1995**, *11*, 4639−4641.
(30) Ogawa, M. *Chem. Commun.* **1996**, 1149−1150.
(31) Ogawa, M. *Langmuir* **1997**, *13*, 1853−1855.
(32) McGrath, K. M.; Dabbs, D. M.; Yao, N.; Aksay, I. A.; Gruner, S. M. *Science* **1997**, *277*, 552−556.
(33) Gangull, Y.; Lu, R.; Drewien, C. A.; Anderson, M. T.; Brinker, C. J.; Gong, W.; Guo, Y.; Soyez, H.; Dunn, B.; Huang, M. H.; Zink, J. I. *Nature* **1997**, *389*, 364−368.
(34) Tagaya, M.; Okuda, M.; Jones, S. W.; Kobayashi, T. *Trans. on GIGAKU* **2012**, *1*, 01012/1−01012/6.
(35) Lin, H.-P.; Mou, C.-Y. *Science* **1996**, *273*, 765−768.
(36) Huo, Q.; Feng, J.; Schüth, F.; Stucky, G. D. *Chem. Mater.* **1997**, *9*, 14−17.
(37) Bruishman, P. J.; Kim, A. Y.; Liu, J.; Baskaran, S. *Chem. Mater.* **1997**, *9*, 2507−2512.
(38) Huo, Q.; Zhao, D.; Feng, J.; Weston, K.; Buratto, S. K.; Stucky, G. D.; Schacht, S.; Schüth, F. *Adv. Mater.* **1997**, *9*, 974−978.
(39) (a) Melosh, N. A.; Lipic, P.; Bates, F. S.; Stucky, G. D.; Wudl, F.; Fredrickson, G. H.; Chmelka, B. F. *Macromolecules* **1999**, *32*, 4332−4342.
(40) Feng, P. Y.; Bu, X. H.; Pine, D. J. *Langmuir* **2000**, *16*, 5304−5310.
(41) Klein, L. C. *Annu. Rev. Mater. Sci.* **1993**, *23*, 437−452.
(42) Scott, B. J.; Wirnsberger, G.; Stucky, G. D. *Chem. Mater.* **2001**, *13*, 3140−3150.
(43) Lu, Y. B.; Franze, K.; Seifert, G.; Steinhäuser, C.; Kirchhoff, F.; Wolburg, H.; Guck, J.; Janmey, P.; Wei, E. Q.; Käs, J.; Reichenbach, A. *Proc. Natl. Acad. Sci. U.S.A.* **2006**, *103*, 17759−17764.
(44) Brunner, C. A.; Ehrlicher, A.; Kohlstrunk, B.; Knebel, D.; Käs, J. A.; Goegler, M. *Eur. Biophys. J.* **2006**, *35*, 713−719.
(45) Singh, C. P.; Yousuf, M.; Qadri, S. B.; Turner, D. C.; Gaber, B. P.; Ratna, B. R. *Appl. Phys. A: Mater. Sci. Process.* **2003**, *77*, 585−589.
(46) Zhao, D.; Sun, J.; Li, Q.; Stucky, G. D. *Chem. Mater.* **2000**, *12*, 275−279.
(47) Melosh, N. A.; Lipic, P.; Bates, F. S.; Wudl, F.; Stucky, G. D.; Fredrickson, G. H.; Chmelka, B. F. *Macromolecules* **1999**, *32*, 4332−4342.
(48) Yamamoto, S.; Yamada, H.; Matsushige, K. *Jpn. J. Appl. Phys.* **2000**, *39*, 3717−3720.
(49) Kendall, K.; Tabor, D. *Proc. Roy. Soc. Lond.* **1971**, *A323*, 321−340.
(50) Soler-Illia, G. J. D. A.; Crepaldi, E. L.; Grosso, D.; Sanchez, C. *Curr. Opin. Colloid Interface Sci.* **2003**, *8*, 109−126.